Int J Thermophys (2007) 28:1628–1645
DOI 10.1007/s10765-007-0239-2

Development and Characterization of Low-Emitting Ceramics

Jochen Manara · M. Reidinger · S. Korder · M. Arduini-Schuster · J. Fricke

Published online: 10 August 2007

Abstract The infrared-optical properties of ceramics are correlated with the complex index of refraction of the material and the structure of the ceramic. By changing these parameters, the infrared-optical properties can be changed over a relatively wide range. The correlation of the structural properties (like the porosity or the pore sizes) and the material properties (such as the complex index of refraction on the one hand and the infrared-optical properties such as emittance on the other) are described by a solution of the equation of radiative transfer and the Mie-theory. Within this work, low-emitting ceramics, which have significantly lower emittances than conventional ceramics, were prepared by optimizing their composition and structure. The spectral emittance of these ceramics was measured, and a total emittance dependent on temperature was calculated from the spectral emittance. As a result, one obtains ceramics which have a total emittance of 0.2 at a temperature of 1,100 K. In comparison to conventional ceramics with a typical total emittance of 0.8 at 1,100 K, the use of such low-e ceramics leads to a reduction in heat transfer of about 70% via thermal radiation. The results of our calculations were compared with experimental data to validate the theory.

Keywords Ceramics · Emittance · Infrared · Low-e · Scattering · Three-flux approximation

Paper presented at the Seventh European Conference on Thermophysical Properties, September 5–8, 2005, Bratislava, Slovak Republic.

J. Manara (✉) · M. Reidinger · S. Korder · M. Arduini-Schuster · J. Fricke
Bayerisches Zentrum für Angewandte Energieforschung e.V. (ZAE Bayern), Am Hubland, 97074 Würzburg, Germany
e-mail: manara@zae.uni-wuerzburg.de

Symbols

μ	Direction cosine
τ	Optical depth
τ_0	Optical thickness
Π	Porosity
θ	Scattering angle (rad)
ε	Total emittance
ε_λ	Spectral emittance
λ	Wavelength (m)
λ_{Chr}	Christiansen wavelength (m)
Ω, Ω'	Solid angle (sr)
ω_0	Albedo
ρ	Powder density ($\mathrm{kg}\cdot\mathrm{m}^{-3}$)
$\rho_{\mathrm{t.d.}}$	Theoretical density ($\mathrm{kg}\cdot\mathrm{m}^{-3}$)
σ_{g}	Geometric mean standard deviation
ψ_j, ζ_j	Ricatti–Bessel functions
ρ_{p}	Internal reflectance
A	Absorption coefficient (m^{-1})
a_i	Weight factors
a_j, b_j	Development coefficients
C_{abs}	Absorption cross-section (m^2)
C_{ext}	Extinction cross-section (m^2)
C_{sca}	Scattering cross-section (m^2)
d	Thickness (m)
D	Diameter (m)
D_{M}	Modal value (m)
E	Extinction coefficient (m^{-1})
F	Radiative flux ($\mathrm{W}\cdot\mathrm{m}^{-1}\cdot\mathrm{m}^{-2}$)
g	Anisotropy factor
I_λ	Spectral intensity ($\mathrm{W}\cdot\mathrm{m}^{-1}\cdot\mathrm{m}^{-2}\cdot\mathrm{sr}^{-1}$)
$I_{\mathrm{b},\lambda}$	Spectral intensity of a blackbody ($\mathrm{W}\cdot\mathrm{m}^{-1}\,\mathrm{m}^{-2}\,\mathrm{sr}^{-1}$)
J	Source term ($\mathrm{W}\cdot\mathrm{m}^{-1}\cdot\mathrm{m}^{-2}\cdot\mathrm{sr}^{-1}$)
k	Imaginary part of the complex refractive index
m	Complex refractive index
m_{particle}	Mass of a powder particle (kg)
m_{total}	Sample mass (kg)
n	Real part of the complex refractive index
N	Number of particles
p	Phase function
Q_{abs}	Efficiency for absorption
Q_{ext}	Efficiency for extinction
Q_{sca}	Efficiency for scattering
R_{dh}	Directional-hemispherical reflectance

R_i	Angular-dependent reflectance
$\overline{R}_i$	Mean internal reflectance
R_p	Reflection of perpendicular beam onto surface
$\mathcal{S}$	Scattering coefficient (m^{-1})
T	Temperature (K)
T_{dh}	Directional-hemispherical transmittance
t_s	Sintering time (s)
T_s	Sintering temperature (K)
V	Sample volume (m^3)
$V_{particle}$	Volume of a powder particle (m^3)
x	Length (m)
z	Size parameter
Subscript:	
*	Effective

1 Introduction

The heat transfer through materials and the heat exchange between surfaces are important in many applications. In automotive applications ceramic coatings with low emittances are desirable. Hot parts, such as the exhaust manifold or the catalytic converter, can be covered with a ceramic coating. Such coatings should have a low emittance to reduce the heat transfer to neighboring parts within the engine compartment [1]. Additionally, ceramics with a low emittance are useful in many applications at high temperatures, where the heat exchange via radiation must be suppressed. In addition to ceramic coatings, monolithic ceramics with low-e properties are also highly interesting.

The total emittance of a ceramic depends on its temperature, as the spectral emittance varies with wavelength. In this work, oxide ceramics are investigated as they are white in the visible and near-infrared regions. This means that the emittance is relatively low for wavelengths below 2 µm. For opaque samples the emittance increases with increasing wavelength and becomes one at the so-called Christiansen wavelength [2]. At the Christiansen wavelength the real part of the refractive index is one, so that no reflection occurs. If the imaginary part of the refractive index is small compared to one, but non-vanishing, and if the thickness of the sample is sufficiently large, no transmittance occurs, and all radiation is absorbed, i.e., the emittance becomes one. For most oxide ceramics, the Christiansen wavelength lies between 8 µm and 16 µm. The Christiansen wavelength depends only on the refractive index of the material. Therefore, no significant variation of the Christiansen wavelength can be achieved by changing the porosity or the structure of the ceramic.

However, the shoulder where the increase of the emittance appears can be shifted toward longer wavelengths by optimizing the porosity and structure of the ceramic. The Christiansen wavelength itself can be shifted toward longer wavelengths by using materials with optimum refractive indices. Therefore, both parameters are varied in this work; the refractive index by changing the material and the structure by changing the parameters within the manufacturing process.

In this work, monolithic samples were produced via a sintering process, as this is the most common method of producing ceramics. The results can also be applied to ceramic coatings, as such coatings can be produced in a similar way, for example, via electrophoretic deposition followed by a sintering process.

2 Radiative Transfer within Porous Media

The propagation of radiation through a porous medium like a ceramic is hindered by scattering and absorption [3,4]. Scattering of radiation mainly occurs at the interface between the medium (for example, the ceramic) and the surrounding medium (mostly air) and at the air-filled pores within the ceramic. The absorption mainly occurs within the ceramic. To reduce the emittance of a ceramic, the scattering has to be maximized and the absorption has to be minimized. The correlation between the scattering and absorption on the one hand, and the complex refractive index $m = n + ik$ and the structure of the medium on the other, are discussed in the following chapters.

The propagation of radiation through a medium with known scattering and absorption coefficients can be described via the equation of radiative transfer. A solution of the equation of radiative transfer is presented in Sect. 2.2. The scattering and absorption coefficients can be calculated from the known refractive index and the pore size distribution within the ceramic using Mie-theory as explained in Sect. 2.3. The definitions of the spectral and total emittance are given in Sect. 2.1.

2.1 Emittance

The emittance $\varepsilon_\lambda(T)$ of a surface at a given temperature is defined as the ratio of the intensity emitted by a surface $I_\lambda(T)$ and the intensity $I_{\mathrm{b},\lambda}(T)$ emitted by a blackbody at the same temperature T:

$$\varepsilon_\lambda = \frac{I_\lambda(T)}{I_{\mathrm{b},\lambda}(T)}. \tag{1}$$

Within this work the term emittance is used instead of emissivity, according to a suggestion from the National Institute of Standards and Technology (NIST). NIST suggests the ending *-ivity* should be reserved for the properties of optically smooth, opaque, and homogeneous materials [5]. However, no emittance can be provided for semitransparent samples, as the emittance of such ceramics is not only a surface property, but also a volumetric property. Additionally, a temperature gradient may occur inside the ceramic. In such cases it is possible to use an apparent emittance, where the intensity $I_\lambda(T)$ in Eq. 1 represents the intensity emitted by the ceramic sample with an average temperature T. For a simpler presentation in this article, the apparent emittance is always called the emittance.

The directional emittance ε_λ can be measured directly or calculated from the directional-hemispherical reflectance R_{dh} and transmittance T_{dh}:

$$\varepsilon_\lambda = 1 - R_{\mathrm{dh}} - T_{\mathrm{dh}}. \tag{2}$$

The total emittance $\varepsilon(T)$ can be calculated from the spectral emittance ε_λ:

$$\varepsilon(T) = \frac{\int_0^\infty \varepsilon_\lambda I_{b,\lambda}(T)\mathrm{d}\lambda}{\int_0^\infty I_{b,\lambda}(T)\mathrm{d}\lambda}. \tag{3}$$

2.2 Equation of Radiative Transfer

The transmission of thermal radiation through semitransparent materials and the emission of radiation from semitransparent materials can be described by the equation of radiative transfer [6], which gives the variation of the spectral intensity I with the path x parallel to the radiation propagation within a plane-parallel sample:

$$\frac{\mathrm{d}I(x)}{\mathrm{d}x} = -EI(x) + \frac{\mathcal{S}}{4\pi}\int_{4\pi} I(x,\Omega')p(x,\Omega',\Omega)\mathrm{d}\Omega' + AI_b(x) + EJ(\tau), \tag{4}$$

where E is the extinction coefficient, $E = A + \mathcal{S}$, A is the absorption coefficient, $\mathcal{S}$ is the scattering coefficient, and $p(\Omega', \Omega)$ is the phase function for the radiation coming from the solid angle Ω' and scattered into the solid angle Ω. $I_b(x)$ gives the intensity emitted by a blackbody. The first term on the right-hand side of Eq. 4 describes the exponential decrease in I caused by scattering and absorption events. The second and third terms characterize the increase in I due to isotropic scattering and re-emission, respectively. The source term $J(\tau)$ accounts for the incoming radiation F that reaches the point τ (optical depth, $\tau = Ex$), if the sample is irradiated normal to the surface (Fig. 1),

$$J(\tau) = \frac{\omega_0 F}{4\pi}\rho_p(\tau) = \frac{\omega_0 F}{4\pi}\frac{1-R_p}{1-{R_p}^2\exp(-2\cdot\tau_0)}\left[\exp(-\tau) + R_p\exp(-2\tau_0+\tau)\right], \tag{5}$$

where

$$R_p(n,k) = \frac{(n-1)^2+k^2}{(n+1)^2+k^2}, \tag{6}$$

is the directional–directional reflectance normal to the surface air—medium and medium—air and $\rho_p(\tau)$ is the internal reflectance, which is given as the sum of the terms in Fig. 1.

Equation 4 can be re-written and simplified for isotropic scattering ($p \equiv 1$):

$$\mu\frac{\mathrm{d}I(\tau)}{\mathrm{d}\tau} = -I(\tau) + \frac{\omega_0}{2}\int_{-1}^{1} I(\tau,\mu')\mathrm{d}\mu' + \frac{A}{E}\frac{n^2\sigma T^4(\tau)}{\pi} + J(\tau), \tag{7}$$

where τ is the optical depth, $\tau = Ex$, ω_0 is the albedo, $\omega_0 = \mathcal{S}/E$, μ is the direction cosine, $\mu = \cos\theta$, and θ is the scattering angle.

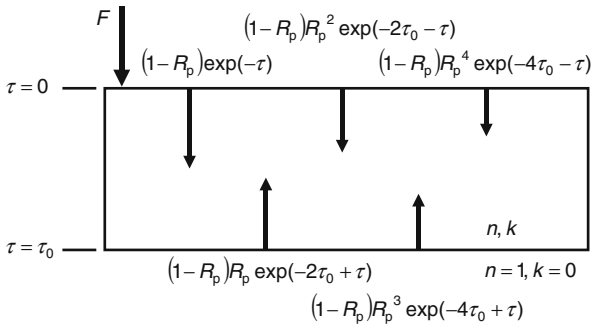

Fig. 1 Multiple reflections of the incoming radiation F, impinging normal to the sample surface. Also given are the reflected parts of the incoming radiation. Summarizing these terms leads to the internal reflectance $\rho_p(\tau)$

The equation of radiative transfer can be solved for isotropic scattering. The transformation of the solution to anisotropic scattering can be made via a scaling concept [7]. In this scaling concept an effective optical thickness τ_0^* and an effective albedo ω_0^* are defined which are correlated to the optical thickness $\tau_0 = Ed$ (d gives the sample thickness) and the albedo ω_0 by the anisotropy factor g;

$$\tau_0^* = \tau_0(1-\omega_0 g) \quad \text{and} \quad \omega_0^* = \frac{\omega_0(1-g)}{1-\omega_0 g}, \tag{8}$$

with

$$g = \int_{4\pi} \cos\theta p(\theta)\mathrm{d}\Omega. \tag{9}$$

The values of the anisotropy factor are within the interval -1 (backward scattering) to +1 (delta function like forward scattering). The effective extinction coefficient E^* is defined analogously (cf. Eq. 25).

Discrete ordinate approximation can be used [8] to solve Eq. 7. For this approximation, the integral in Eq. 7 is transformed into a sum over a few intensities. Three discrete directions are regarded for the three-flux approximation:

$$\int_{-1}^{1} I(\tau^*, \mu')\mathrm{d}\mu' \to \sum_{j=-1}^{1} a_j I_j. \tag{10}$$

The direction cosines of these directions are determined from the weight factors a_j of the intensities I_j to [8]

$$\mu_{-1} = -\frac{2}{3}, \quad \mu_0 = 0, \quad \mu_1 = \frac{2}{3}. \tag{11}$$

The boundary conditions are

$$I_1(\tau^* = 0) = \overline{R}_\mathrm{i} I_{-1}(\tau^* = 0), \tag{12}$$
$$I_{-1}(\tau^* = \tau_0^*) = \overline{R}_\mathrm{i} I_1(\tau^* = \tau_0^*). \tag{13}$$

The mean internal reflectance $\overline{R}_\mathrm{i}$ can be determined from the angular-dependent reflectance R_i:

$$\overline{R}_\mathrm{i}(n,k) = \frac{\int_0^1 \mu R_\mathrm{i}(\mu,n,k)\mathrm{d}\mu}{\int_0^1 \mu \mathrm{d}\mu} = 2\int_0^1 \mu R_\mathrm{i}(\mu,n,k)\mathrm{d}\mu. \tag{14}$$

It represents that part of the scattered radiation which hits the interface medium–air from all directions and is reflected back into the medium. Mathematically, the three-flux approximation has the same complexity as the two-flux approximation, but provides far better accuracy [9].

Finally, one obtains the macroscopic values of the directional-hemispherical reflectance R_dh and transmittance T_dh as a function of the microscopic values, the effective extinction coefficient E^*, the effective albedo ω_0^*, and the complex refractive index $m = n + ik$ of the medium:

$$T_\mathrm{dh} = \frac{(1-\overline{R}_\mathrm{i})I_{+1}(\tau^* = \tau_0^*, \omega_0^*) + \frac{F}{\pi}\frac{(1-R_\mathrm{p})^2}{1-R_\mathrm{p}{}^2\exp(-2\tau_0^*)}\exp(-\tau_0^*)}{\frac{F}{\pi}}, \tag{15}$$

$$R_\mathrm{dh} = \frac{(1-\overline{R}_\mathrm{i})I_{-1}(\tau^* = 0, \omega_0^*) + \frac{F}{\pi}R_\mathrm{p} + \frac{F}{\pi}\frac{(1-R_\mathrm{p})^2 R_\mathrm{p}\exp(-2\tau_0^*)}{1-R_\mathrm{p}^2\exp(-2\tau_0^*)}}{\frac{F}{\pi}}. \tag{16}$$

When measuring the reflectance and transmittance of the sample, the re-emission term in Eq. 4 can be neglected as the incoming radiation is modulated by the FTIR-technique, whereas the emitted radiation is not modulated. To calculate the radiation emitted from the sample as a function of the sample temperature, the boundary conditions have to be modified and the source term in Eq. 4 can be neglected as no incoming radiation has to be considered.

2.3 Mie-Theory

Mie-theory gives a description of the scattering of an electromagnetic plane wave at a spherical particle. This theory is named after Gustav Mie, who first published it in 1908 [10]. For spheres, the Maxwell equations can be solved exactly. The whole procedure is described in detail in Refs. 11–13. As a result of these calculations, one gets the so-called development coefficients a_j and b_j, which are determined by the

Ricatti–Bessel functions ψ_j, ζ_j, and their derivatives ψ'_j, ζ'_j [12]:

$$a_j = \frac{\psi'_j(m_{\text{air}}z)\psi_j(mz) - \frac{m_{\text{air}}}{m}\psi_j(m_{\text{air}}z)\psi'_j(mz)}{\psi'_j(m_{\text{air}}z)\zeta_j(mz) - \frac{m_{\text{air}}}{m}\psi_j(m_{\text{air}}z)\zeta'_j(mz)}, \tag{17}$$

$$b_j = \frac{\frac{m_{\text{air}}}{m}\psi'_j(m_{\text{air}}z)\psi_j(mz) - \psi_j(m_{\text{air}}z)\psi'_j(mz)}{\frac{m_{\text{air}}}{m}\psi'_j(m_{\text{air}}z)\zeta_j(mz) - \psi_j(m_{\text{air}}z)\zeta'_j(mz)}. \tag{18}$$

m_{air} gives the complex refractive index of the pores, which are filled with air, and m gives the complex refractive index of the solid ceramic. The Ricatti–Bessel functions ψ_j and ζ_j are defined by the spherical Bessel and Hankel functions j_j and h_j [11]:

$$\psi_j(v) = vj_j(v), \quad \zeta_j(v) = vh_j^{(1)}(v). \tag{19}$$

The definitions of the spherical Bessel and Hankel functions are given, for example, in Ref. 14.

Finally, one gets the absorption and scattering coefficients of spheres as a function of the complex refractive indices m_{air}, m, and the size parameter z:

$$z = \frac{\pi D}{\lambda}, \tag{20}$$

where D is the particle diameter and λ is the wavelength of the incoming radiation. The Mie-theory is only valid for spherical particles, but reliable results [11] can be obtained even for non-spherical particles. In porous ceramics mainly the air-filled pores embedded in the solid ceramic with its complex refractive index m are responsible for scattering radiation.

The scattering cross-section C_{sca} and the absorption cross-section C_{abs} are defined as the quotient of the scattered or absorbed radiant power and the incoming intensity, respectively. By dividing the scattering and absorption cross-sections by the geometrical cross-section, one gets the efficiency for scattering Q_{sca} and absorption Q_{abs}, which are determined by the development coefficients a_j and b_j [12]:

$$\begin{aligned} Q_{\text{sca}} &= \frac{C_{\text{sca}}}{\pi\left(\frac{D}{2}\right)^2} = \frac{2}{z^2}\sum_{j=1}^{\infty}(2j+1)\left(|a_j|^2 + |b_j|^2\right) \\ Q_{\text{ext}} &= \frac{C_{\text{ext}}}{\pi\left(\frac{D}{2}\right)^2} = \frac{2}{z^2}\sum_{j=1}^{\infty}(2j+1)\text{Re}\left(a_j + b_j\right). \\ Q_{\text{abs}} &= Q_{\text{ext}} - Q_{\text{sca}} \end{aligned} \tag{21}$$

The efficiency for extinction Q_{ext} is defined as the sum of the efficiency for scattering and absorption.

The scattering within a powder occurs at the powder-particles, which means at the air–medium interfaces, whereas the scattering inside a ceramic occurs at the air-filled pores, which means at the medium–air interfaces (Fig. 2), as mentioned above.

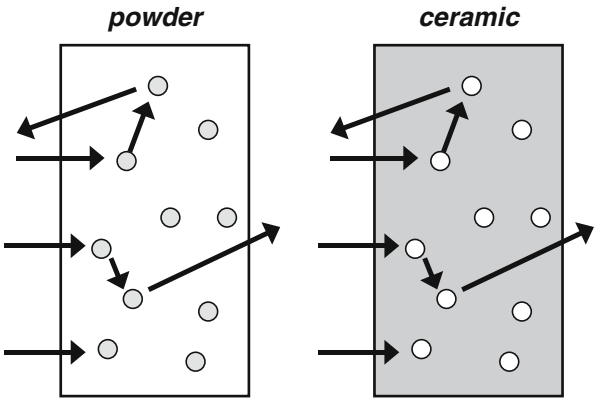

Fig. 2 Within a powder, scattering occurs mainly at the powder-particles (shown on the left), whereas inside a ceramic, scattering occurs mainly at the air-filled pores (shown on the right)

Both cases can be described with Mie-theory; only the refractive indices need to be changed. The extinction coefficient of a powder E_{powder} for independent scattering and absorption events is defined as

$$E_{\text{powder}} = \frac{N}{V} C_{\text{ext}} = \frac{m_{\text{total}}}{m_{\text{particle}}} \frac{1}{V} Q_{\text{ext}} \pi \left(\frac{D}{2}\right)^2 = \frac{\rho V}{\rho_{\text{t.d.}} V_{\text{particle}}} \frac{1}{V} Q_{\text{ext}} \pi \left(\frac{D}{2}\right)^2 = \frac{3}{2} \frac{\rho}{\rho_{\text{t.d.}}} \frac{Q_{\text{ext}}}{D} \tag{22}$$

In Eq. 22 N/V represents the number of particles N per sample volume V. m_{total} gives the total mass of the powder, and m_{particle} represents the mass of one particle. ρ is the density of the powder, $\rho_{\text{t.d.}}$ is the theoretical density or bulk density of the material, and V_{particle} is the volume of one spherical particle with diameter D.

The extinction coefficient E of a porous ceramic can be derived analogously using the porosity Π of the sample instead of the quotient $\rho/\rho_{\text{t.d.}}$. Finally the extinction coefficient E and the scattering coefficient S for a given pore diameter D are expressed as [15]:

$$E(\lambda) = \frac{3}{2} \Pi \frac{Q_{\text{ext}}(\lambda)}{D}, \quad \mathcal{S}(\lambda) = \frac{3}{2} \Pi \frac{Q_{\text{sca}}(\lambda)}{D}. \tag{23}$$

The anisotropy factor g is also determined by the development coefficients a_j and b_j, [16]:

$$g = \frac{4}{z^2 Q_{\text{sca}}} \sum_{j=1}^{\infty} \left[\frac{j(j+2)}{j+1} \text{Re}\left(a_j \overline{a}_{j+1} + b_j \overline{b}_{j+1}\right) + \frac{2j+1}{j(j+1)} \text{Re}(a_j \overline{b}_j) \right]. \tag{24}$$

With the anisotropy factor, the effective efficiency for extinction Q^*_{ext} and scattering Q^*_{sca} can be derived as well as the effective extinction and scattering coefficients E^*

Table 1 Data for the monolithic ceramic samples prepared at ZAE Bayern (samples have a diameter of about 30 mm)

Sample No.	Material	Thickness d (mm)	Sintering temperature T_s (K)	Sintering time t_s (h)	Porosity Π
1	HfO_2	1.3	1473	1	0.39
2	Al_2O_3	4.0	1973	8	0.02
3	Al_2O_3	3.7	1873	6	0.27
4	TiO_2	1.3	1873	8	0.01
5	TiO_2	2.3	1373	6	0.42
6	Y_2O_3	2.1	1873	6	0.17
7	Y_2O_3	2.4	1773	2	0.37

and $\mathcal{S}^*$:

$$\begin{aligned} Q^*_{\text{ext}} &= Q_{\text{ext}}(1-\omega_0 g), \quad E^* = E(1-\omega_0 g) \\ Q^*_{\text{sca}} &= Q_{\text{sca}}(1-g), \quad \mathcal{S}^* = \mathcal{S}(1-g). \end{aligned} \tag{25}$$

Normally, one has not only pores with a given diameter D, but also a pore size distribution. Often one assumes that the pore volume within a logarithmic diameter interval $\Delta \ln D$ is distributed like a logarithmic normal distribution [12]:

$$f(D)\Delta \ln D = \frac{1}{\sqrt{2\pi}\sigma_g} \exp\left[-\frac{(\ln D - \ln D_M)^2}{2\sigma_g^2}\right] \Delta \ln D. \tag{26}$$

The modal value D_M and the geometric mean standard deviation σ_g can be calculated by a least-squares fit with the measured spectral effective extinction coefficient E^*_{exp} and the spectral effective extinction coefficient E^* calculated from Eqs. 23 and 25.

3 Sample Production and Experimental Setup

The monolithic samples characterized in this work were made via a sintering process at ZAE Bayern. First, the ceramic powders were pressed at 100 MPa. Then the green bodies obtained were sintered at different temperatures and with different sintering times. The porosities of the samples were measured using the Archimedes principle. The resulting data of the produced sample slides, which have a diameter of about 30 mm, can be seen in Table 1. Additionally, several SEM (scanning electron microscope) images of the samples were made.

The ceramic coating presented in this work was prepared at the German Aerospace Center (DLR) via EB-PVD (electron-beam physical-vapor deposition) as explained in Ref. 17.

The directional-hemispherical transmittance T_{dh} of both the ballistic transmitted radiation and the diffusely scattered radiation at the back of the sample was measured using an integrating sphere (Fig. 3) [18]. The directional-hemispherical reflectance R_{dh} can also be measured with an integrating sphere. For the wavelength range from 0.25 to 2.5 µm, a Perkin Elmer lambda nine diffraction-spectrometer was used and for

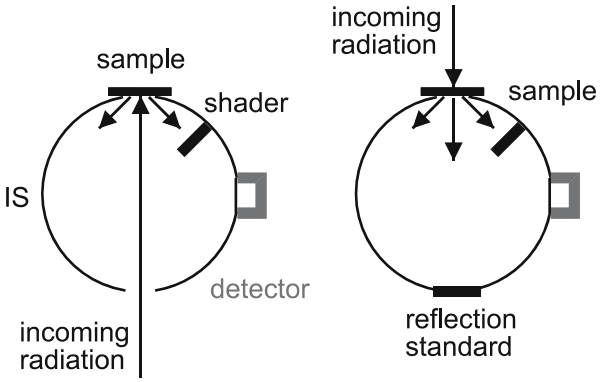

Fig. 3 Measurement setups (directional-hemispherical reflectance on the left and directional-hemispherical transmittance on the right) with an integrating sphere (IS). Internal surface of the integrating sphere is coated with a highly reflecting coating which reflects the radiation diffusely

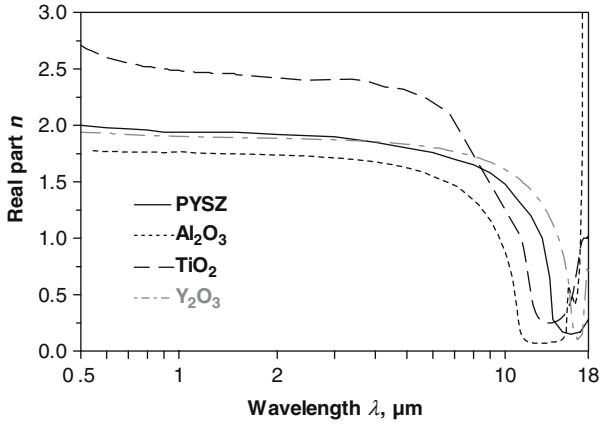

Fig. 4 Real part n of the complex refractive index of several ceramics as a function of wavelength λ from 0.5 to 18 µm at ambient temperature

the wavelength range from 1.4 to 18 µm, a Bruker IFS 66v FTIR-spectrometer was used.

4 Results and Analysis

The real part n and the imaginary part k of the complex refractive index m of the materials investigated in this work are depicted in Figs. 4 and 5, respectively. The data were taken from the literature [19,20] and used in the calculations described above.

The directional-hemispherical reflectance R_{dh} and transmittance T_{dh} of the samples were measured. Samples with different thicknesses were produced. Samples with a vanishing transmittance were produced to determine the emittance. Additionally, samples with a non-vanishing transmittance were made to analyze the structure.

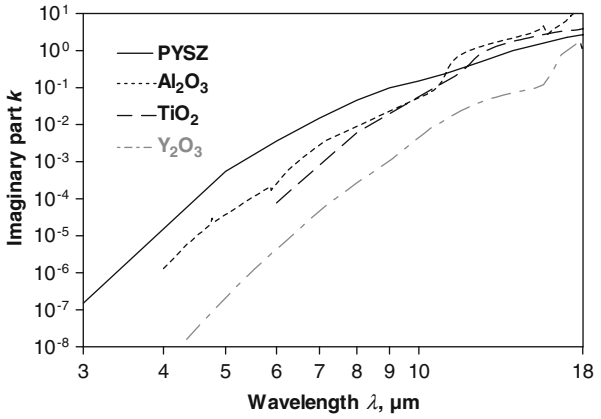

Fig. 5 Imaginary part k of the complex refractive index of several ceramics as a function of wavelength λ from 3 to 18 µm at ambient temperature, note the logarithmic ordinate

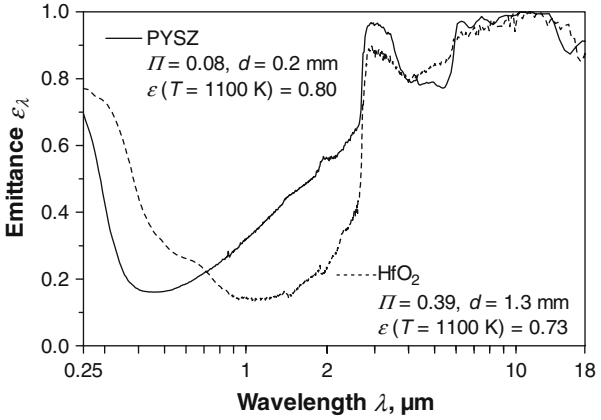

Fig. 6 Directional emittance ε_λ of partially yttria stabilized zirconia (PYSZ) and hafnium oxide as a function of wavelength λ from 0.25 to 18 µm at ambient temperature

First, the emittance was determined from the samples with vanishing transmittance. The emittance of conventional coatings, such as a thermal barrier coating made of PYSZ (partially yttria stabilized zirconia), is relatively high. The spectral emittance of one PYSZ-coating is depicted in Fig. 6. The total emittance at 1,100 K is 0.8. The spectral emittance of hafnium oxide (a conventional monolithic ceramic), also depicted in Fig. 6, has a total emittance of 0.73, which is only slightly smaller. Although not often used, hafnium oxide has almost the same properties as zirconia, which is used in a wide range of applications.

Like most oxide ceramics, both ceramics have a low emittance in the visible wavelength region. Therefore, they appear white. But with increasing wavelength, the emittance increases and becomes one at the so-called Christiansen wavelength. For PYSZ and hafnium oxide, the Christiansen wavelength lies at 13 µm, independent of the structure.

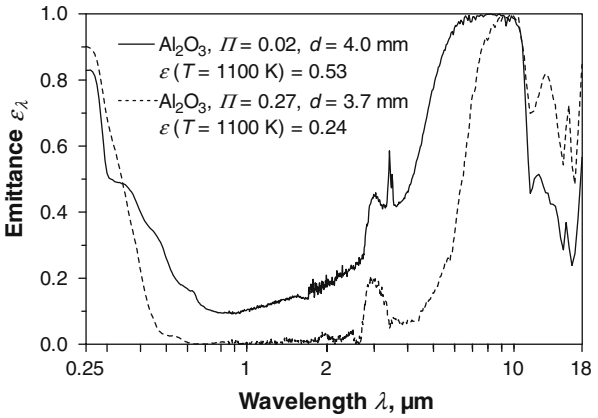

Fig. 7 Directional emittance ε_λ of alumina as a function of wavelength λ from 0.25 to 18 µm at ambient temperature

By changing the structure, it is possible to shift the slope of the emittance towards longer wavelengths. This is demonstrated in Fig. 7 for alumina. The total emittance at 1,100 K of a sample with a porosity of 0.02 is 0.53. By increasing the porosity, the total emittance can be decreased to 0.24. This is due to the fact that the spectral emittance is reduced, especially between 2 µm and 8 µm.

Due to a higher imaginary part of the refractive index, the same procedure does not lead to a significant reduction in the spectral emittance of hafnium oxide, although the Christiansen wavelength of alumina lies at 10 µm and is therefore lower than the Christiansen wavelength of hafnium oxide. As a consequence, both parameters need to be optimized—the material with its refractive index and the structure of the material.

TiO_2 has a higher Christiansen wavelength (at 12 µm) than Al_2O_3 and a higher refractive index than HfO_2 and ZrO_2. Therefore, the total emittance at 1,100 K is lower than for the named materials. The spectral emittance for two TiO_2 samples is depicted in Fig. 8. The resulting total emittance at 1,100 K is 0.34 for a porosity of 0.01 and 0.27 for a porosity of 0.42.

In Fig. 9, the spectral emittance of yttria is plotted for different porosities. The Christiansen wavelength lies at 15 µm. Because of that and the fact that yttria has the smallest imaginary part of the investigated materials, the emittance at 1,100 K is smaller than for the other ceramics characterized in this work. The emittance can be reduced additionally by varying the structure. For a porosity of 0.17, one gets an emittance of 0.19 at 1,100 K. If the porosity is further increased, the total emittance also increases. Therefore, an optimum of the structure and porosity exists at which the total emittance has a minimum. The Christiansen wavelength and the total emittance at 1,100 K for all samples are shown in Table 2.

To correlate the structure and the total emittance, SEM (scanning electron microscope) images of the samples were taken. SEM images of samples 4, 5, and 6 are shown in Figs. 10, 11, and 12, respectively. The porosity of sample 4 (TiO_2) is very low ($\Pi = 0.01$); therefore, the dimensions of the structure are about 50 µm. Due to the relatively large real part of the refractive index, a total emittance of 0.34 results at

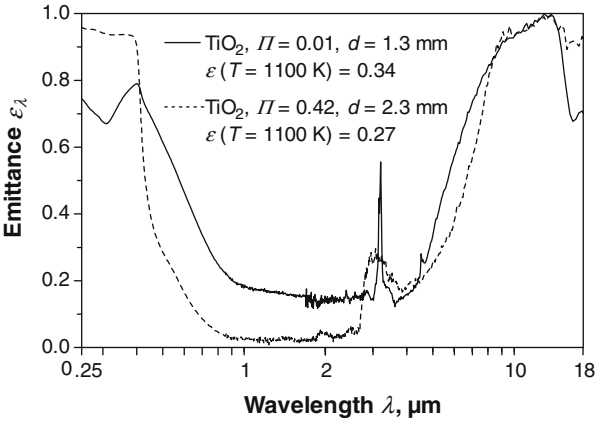

Fig. 8 Directional emittance ε_λ of titania as a function of wavelength λ from 0.25 to 18 µm at ambient temperature

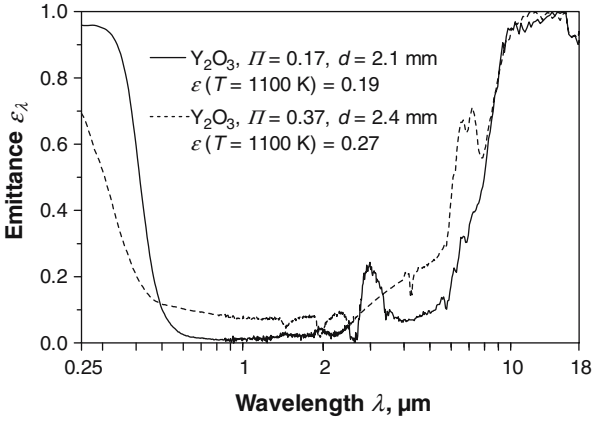

Fig. 9 Directional emittance ε_λ of yttria as a function of wavelength λ from 0.25 to 18 µm at ambient temperature

Table 2 Christiansen wavelength λ_{Chr} and total emittance $\varepsilon(T)$ of the monolithic ceramic samples measured at ZAE Bayern

Sample No.	Material	Christiansen wavelength λ_{Chr} (µm)	Total emittance $\varepsilon(T)$ at $T = 1,100$ K
1	HfO_2	13	0.73
2	Al_2O_3	10	0.53
3	Al_2O_3	10	0.24
4	TiO_2	12	0.34
5	TiO_2	12	0.27
6	Y_2O_3	15	0.19
7	Y_2O_3	15	0.27

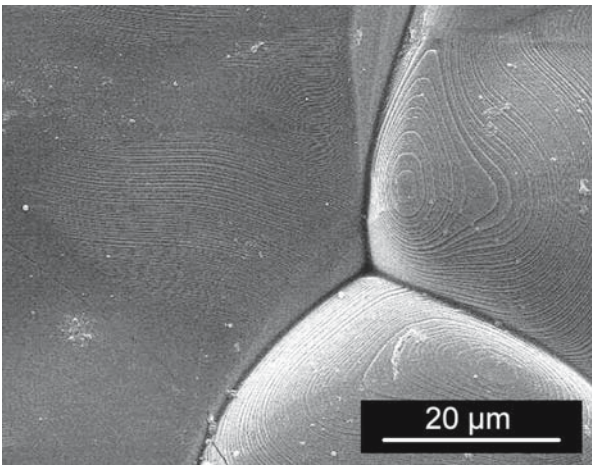

Fig. 10 SEM image (enlargement factor = 2000) taken of sample 4 (TiO_2 with $\Pi = 0.01$)

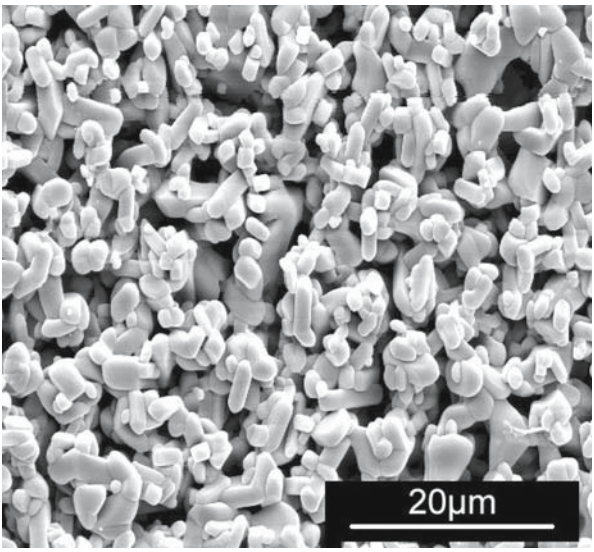

Fig. 11 SEM image (enlargement factor = 2000) taken of sample 5 (TiO_2 with $\Pi = 0.42$)

1,100 K. With a lower sintering temperature and smaller time, one gets a significantly higher porosity ($\Pi = 0.42$) with a finer structure (sample 5) and dimensions of about 3 µm. This results in a lower total emittance of 0.27. Sample 6 (Y_2O_3 with $\Pi = 0.17$) has a structure with dimensions of about 1 µm and a total emittance of 0.19. This is due to the structural properties and the Christiansen wavelength, which lies at a longer wavelength compared to TiO_2.

To obtain more information about the structure of sample 6, the directional-hemispherical reflectance and transmittance were measured for a thinner sample prepared

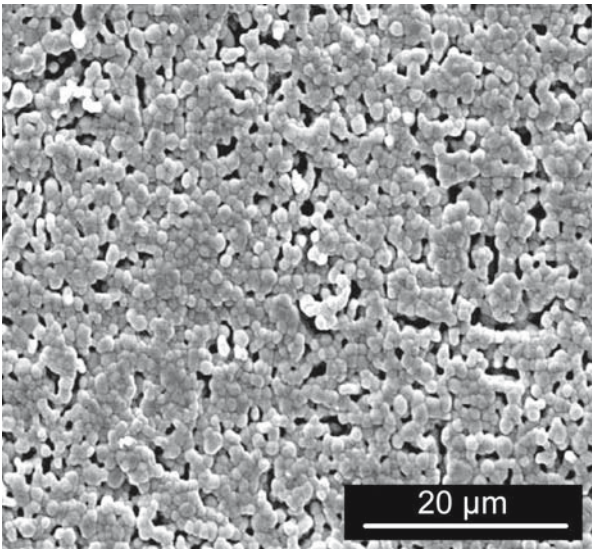

Fig. 12 SEM image (enlargement factor = 2000) taken of sample 6 (Y_2O_3 with $\Pi = 0.17$)

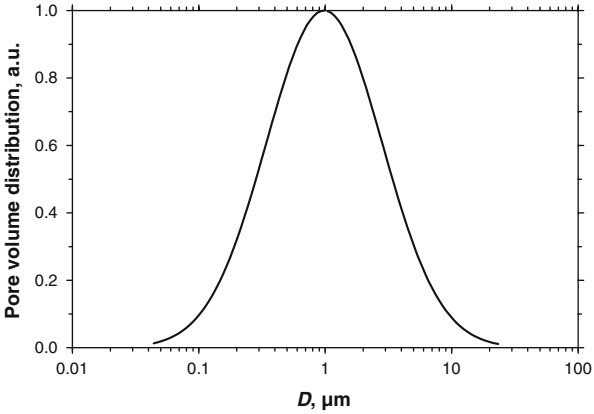

Fig. 13 Pore volume distribution of sample 6 (Y_2O_3 with $\Pi = 0.17$) determined via scattering of radiation inside the ceramic

and sintered together with sample 6 so that both samples have the same properties, except for the thickness.

The effective optical thickness and the effective albedo, which are equivalent to the effective extinction coefficient and effective scattering coefficient, are determined using Eqs. 15 and 16. The dimensions of the structure (Eq. 26) were calculated from the known effective scattering coefficient using Mie-theory. The resulting structural properties are depicted in Fig. 13. Although spherical pores were assumed as scattering centers, the resulting dimensions agree well with the SEM images. Because of this, the pore volume distribution in Fig. 13 gives the distribution of the structural dimensions.

Investigations on the correlation between the structure and the porosity on the one hand and the thermal conductivity on the other will be a topic of future work. In general, a reduction of the thermal conductivity with increasing porosity would be expected.

5 Conclusions

It was shown that the infrared-optical properties of oxide ceramics can be varied over a relatively wide range by varying the material and the structure of the sample. Some of the most promising materials were investigated in this work. As a result the emittance was reduced from 0.80 to 0.19 by optimizing the manufacturing process. One requirement for lowering the emittance is the usage of a material with a large real part and a small imaginary part of the complex refractive index. A second requirement is the optimal structure of the produced sample. The dimensions of the structure should have the same order of magnitude or be slightly smaller than the wavelength of the incoming radiation to get maximal reflectance and therefore minimal emittance.

In this work preliminary investigations were carried out to check the potential reductions in the emittance of ceramics. As these investigations were successful, work is planned to further reduce the emittance, e.g., to achieve an emittance below 0.1 at 1,100 K. In the future, mixtures of different materials with variations of the structure will be investigated. For example, a mixture of titania and yttria is promising, as it unites the large real part of the refractive index of titania with the small imaginary part of the refractive index of yttria. As the refractive index of mixtures can differ significantly from the refractive index of the raw material, a detailed analysis of the mixtures will be necessary.

References

1. A. Knote, H.G. Krüger, H. Kern, J. Manara, *Presented at Thüringer Werkstofftag 2004* (2004)
2. J. Manara, *Infrarot-optischer Strahlungstransport zur Analyse der Struktur und der Wärmeleitfähigkeit von Keramiken für Hochtemperaturanwendungen* (Dissertation zur Erlangung des naturwissenschaftlichen Doktorgrades der Bayerischen Julius-Maximilians- Universität Würzburg, 2001)
3. J. Manara, R. Caps, F. Raether, J. Fricke, Opt. Commun. **168**, 237 (1999)
4. J. Manara, R. Caps, J. Fricke, Int. J. Thermophys. **26**, 531 (2005)
5. R. Siegel, J.R. Howell, *Thermal Radiation – Heat Transfer* (McGraw-Hill, Washington, 1981)
6. T. Burger, J. Kuhn, R. Caps, J. Fricke, Appl. Spectrosc. **51**, 309 (1997)
7. B.H.J. McKellar, M.A. Box, J. Atmos. Sci. **38**, 1063 (1981)
8. M.G. Kaganer, Opt. Spectrosc. **26**, 443 (1969)
9. S. Chandrasekhar, *Radiative Transfer* (Dover Pubs., New York, 1960)
10. G. Mie, Ann. Phys. **25**, 377 (1908)
11. C.F. Bohren, D.R. Huffmann, *Absorption and Scattering of Light by Small Particles* (John Wiley & Sons, New York, 1983)
12. M. Kerker, *The Scattering of Light and Other Electromagnetic Radiation* (Academic Press, Orlando, 1969)
13. H.C. van de Hulst, *Light Scattering by Small Particles* (Dover Pubs., New York, 1981)
14. G. Berendt, E. Weimar, *Mathematik für Physiker, Band 2: Funktionentheorie, gewöhnliche und partielle Differentialgleichungen* (VCH Verlagsgesellschaft mbH, Weinheim, 1990)

15. R. Caps, *Strahlungsströme in evakuierten thermischen Superisolationen* (Dissertation zur Erlangung des naturwissenschaftlichen Doktorgrades der Bayerischen Julius-Maximilians-Universität Würzburg, 1985)
16. H.C. Hottel, A.F. Sarofim, *Radiative Transfer* (McGraw-Hill, New York, 1967)
17. J. Manara, R. Brandt, J. Kuhn, J. Fricke, T. Krell, U. Schulz, M. Peters, W.A. Kaysser, High Temp. – High Press. **32**, 361 (2000)
18. T. Burger, J. Fricke, J. Kuhn, Near Infrared Spectrosc. **6**, 33 (1998)
19. E.D. Palik, *Handbook of Optical Constants of Solids* (Academic Press, San Diego, 1998)
20. H. Tanaka, S. Sawai, K. Morimoto, K. Hisano, J. Therm. Anal. Calorim. **64**, 867 (2001)